LANGMUIR

Article

pubs.acs.org/Langmuir

Study of Compression-Induced Supramolecular Nanostructures of an Imidazole Derivative by Langmuir–Blodgett Technique

Bapi Dey,[†] Pintu Debnath,[†] Santanu Chakraborty,[‡] Barnali Deb,[§] Debajyoti Bhattacharjee,[†] Swapan Majumdar,[§] and Syed Arshad Hussain*[,†]

[†]Thin Film and Nanoscience Laboratory, Department of Physics, and [§]Department of Chemistry, Tripura University, Suryamaninagar, Agartala 799022, West Tripura, Tripura, India

[‡]Department of Physics, NIT Agartala, Jiraniya, Agartala 799046, West Tripura, Tripura, India

Supporting Information

ABSTRACT: In this communication, we report the design and synthesis as well as the supramolecular assembly behavior of a 2,4,5-triaryl imidazole derivative (compound **1**) at the air–water interface and in thin films using Langmuir–Blodgett (LB) technique. The main idea for such a chemical structure is that the long alkyl chain and N–H of the imidazole core may help to form supramolecular architecture through the hydrophobic–hydrophobic interaction and hydrogen bonding, respectively. Accordingly, the interfacial behavior as well as morphology of **1** in thin films were studied through a series of characterization methods such as surface pressure–area (π–A) isotherm, hysteresis analysis, ultraviolet–visible (UV–vis) absorption and steady-state fluorescence spectroscopies, Fourier transform infrared, X-ray diffraction, Brewster angle microscopy (BAM), and atomic force microscopy (AFM) measurements, and so forth. Pressure–area isotherm is an indication toward the formation of supramolecular nanostructures instead of an ideal monolayer at the air–water interface. This has been confirmed by the hysteresis analysis and BAM measurement at the air–water interface. AFM images of **1** in the LB monolayer exhibits the formation of supramolecular nanowires as well as nanorods. By controlling different film-forming parameters, it becomes possible to manipulate these nanostructures. With the passage of time, the nanowires come close to each other and become straight. Similarly, nanorods come close to each other and form bundles of several rods in the LB films. H-bonding, J-aggregation, as well as compression during film formation might play a key role in the formation of such nanostructures. Electrical switching behavior of compound **1** was also observed because of the presence of an electron donor–acceptor system in **1**. This type of organic switching behavior may be promising for next-generation organic electronics.

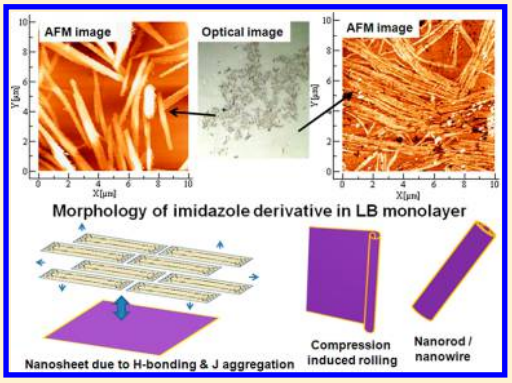

INTRODUCTION

Electronic and optoelectronic devices[1−7] impact many areas of modern society from simple household appliances to communications and sophisticated medical instruments. Given the demand for ever more compact and powerful systems, there is growing interest in the development of nanoscale devices that can enable new functions and/or have greatly enhanced performance. Recent extensive studies have shown that organic nanomaterials exhibit a variety of interesting optical, electrical, photoelectric, and magnetic properties in the solid state. Accordingly, photo- and electroactive organic materials have been the subject of current research,[8−10] including organic semiconductors, organic metals, organic superconductors, organic photoconductors, organic photoactive materials for solar cells, organic nonlinear optical materials, liquid crystals, and others. In addition, organic materials have found a number of potential applications for use in electronic and optoelectronic devices,[11−14] such as sensors, plastic batteries, solar cells, field-effect transistors (FETs), optical data storage, organic electroluminescent devices (OLEDs), switching devices, and so forth. Over the last few decades, tremendous progress has been made in the development and investigation of such new organic materials[15−19] with a readily polarizable structure for the fabrication of novel devices. A conjugated π-system end-capped with a strong electron donor group, such as $-NR_2$ and OR, and a strong electron acceptor group, such as $-NO_2$, cyano (CN), or imine (C═NR), in a molecule generates a dipolar push–pull system (D–π–A) that assures intramolecular charge transfer and low energy barrier and shows an intense charge-transfer band. The extent of electronic or optoelectronic behavior depends primarily on their chemical structure, high chemical and thermal robustness, good solubility in common organic solvents, and availability in reasonable quantities. Hence, various five- and six-membered heterocycles are utilized as suitable π-conjugated chromophore backbones because they act as auxiliary donors or acceptors and

Received: May 24, 2017
Revised: July 27, 2017
Published: August 9, 2017

DOI: 10.1021/acs.langmuir.7b01750
Langmuir 2017, 33, 8383–8394

improve the overall polarizability of the chromophore.[20−23] In this respect, five-membered diazoles, in particular imidazole, seems to be suitable for parent π-conjugated backbones. Imidazole possesses two nitrogen atoms of different electronic nature, represents a robust and stable heterocycle, and can easily be synthesized and further functionalized at positions of the imidazole core.[24−26] In view of the above-mentioned structural features and having in mind the utility of thin films in making devices, we have designed and synthesized 2,4,5-triaryl imidazole derivative **1** having a long alkoxy chain in the 4-position of the aryl group located at C-2 of the imidazole core (Figure 1).[27] The idea is that the oxygen atom in position 4 can

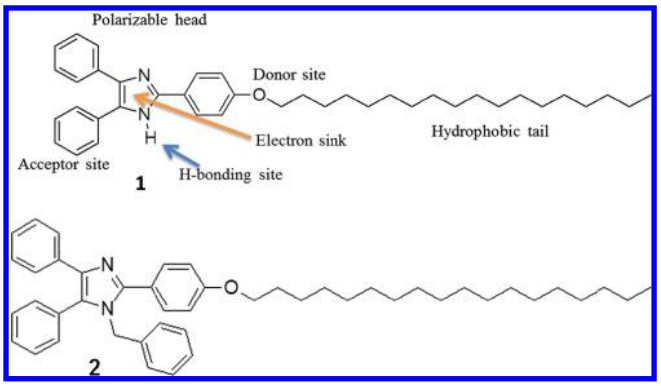

Figure 1. Chemical structure of 2,4,5-triaryl imidazole derivative (**1**) and 1-benzyl-2,4,5-triaryl imidazole derivative (**2**).

act as an electron donor and the C═N group in the imidazole core or other phenyl aryls at C-4 or 5 can act as an electron acceptor, and therefore it is expected that some sort of polarization may occur within the molecule in a particular environment. The long alkyl chain and N−H of the imidazole core will help to form supramolecular architecture through the hydrophobic−hydrophobic interaction and intermolecular association through hydrogen bonding, respectively.

Nanofabrication using the Langmuir−Blodgett (LB) technique provides a useful platform to construct supramolecular functional materials at the air−water interface and onto thin films.[28−32] Here, the monolayer or multilayer of supramolecular assemblies can be formed via the bottom-up assembly.[33−35] Using the LB technique, not only the molecular orientation but also the molecular arrangement as well as the nature of molecular aggregation can be tuned to a certain extent in a two-dimensional manner.[36,37] It is the LB technique, which triggers us to dream about molecular electronics where the organic molecules will perform an active function in the processing and transmission of information as well as storage.

Since its inception, LB technique has been used for the fabrication of uniform mono/multilayer thin films using amphiphilic molecules.[36] However, recent studies have revealed that the LB technique can also be used to prepare other sophisticated morphologies, such as vesicles or nanotubes, nanorods, nanostripes, nanofibers, and their arrays.[37,38] These complex structures in LB films are very important because of their unique photophysical and photochemical properties. Application of nanostructures prepared by supramolecular interfacial assembly toward photodynamic therapy/antitumor therapy has already been demonstrated.[39−42] Layer-by-layer self-assembled diamond-based core−shell nanocomposites have been found as highly efficient dye absorbents for wastewater treatment.[43] It is hardly possible to form such complex structures using conventional amphiphiles in LB films.[44] Specially designed molecules with a suitable architecture and functional group can only form such interesting complex nanostructures onto thin films using the LB technique.[45] There are few reports of nanotubes and nanorods of organic molecules at the air−water interface and in LB films because of the compression-induced rolling of a nanosheet.[45−47] Both chiral as well as achiral molecules were found to form such nanostructures. A series of rod−coil molecules consisting of the imidazole moiety were found to form nanowire/nanorod-like structures because of chirality and formation of J-aggregates in LB films.[48] Various kinds of nanostructures of a series of different Schiff base amphiphiles due to supramolecular assembly using the LB technique have also been reported.[49−53] It was also observed that the imidazole derivative became chiral in LB films when coordinated with a silver ion and formed supramolecular nanostructures.[54] In that respect, it would be interesting to study the supramolecular assembly of **1** at the air−water interface and in thin films using the LB technique.

In this manuscript, we report the design of an important imidazole derivative **1** and the investigation of its supramolecular organization at the air−water interface and in thin films using the LB technique. Compression-induced nanorod- and nanowire-like structures were formed in the LB film. Hydrogen bonding and aggregation at the air−water interface and in the solid substrate played a key role in forming such a nanostructure. The interfacial behavior as well as morphology in the thin film were studied through a series of characterization methods such as surface pressure−area (π−*A*) isotherm, hysteresis analysis, ultraviolet−visible (UV−vis) absorption and steady-state fluorescence spectroscopies, Fourier transform infrared (FTIR), X-ray diffraction (XRD), Brewster angle microscopy (BAM), and atomic force microscopy (AFM) measurements, and so forth. These studies are important to have an idea about the formation mechanism as well as the condition of formation of such supramolecular nanostructures using the LB technique. Although supramolecular nanostructures in a thin film using organic molecules are very important for many potential applications because of their unique properties, very few works have been reported till now.

EXPERIMENTAL SECTION

Materials. Benzil, ammonium acetate, and 4-hydroxybenzaldehyde were purchased from Spectrochem Pvt. Ltd. 1-Bromooctadecane, benzyl bromide, and HBF_4 were purchased from Across Organics. Ammonium acetate, ethyl acetate, dimethylformamide (DMF), and anhydrous K_2CO_3 were purchased from Fisher Scientific, India. Working solutions were prepared by dissolving them in spectroscopic grade chloroform (SRL, India). These materials were used as received.

Synthesis of 2-(4-*O*-Octadecyloxyphenyl)-4,5-diphenyl Imidazole (1). A mixture of benzil (2 mmol), 4-*O*-octadecyloxy benzaldehyde (2 mmol), ammonium acetate (5 mmol), and HBF_4−SiO_2 (0.08 g, contains 2 mol % of HBF_4) was heated until the disappearance of starting materials [thin-layer chromatography (TLC)]. After completion of the reaction, the solid product along with the catalyst was filtered. The catalyst was recovered by dissolving the product in ethyl acetate and washing with the same. The concentration of the solution containing the product was followed by recrystallization from ethanol to afford the corresponding substituted imidazole product, 2-(4-*O*-octadecyloxyphenyl)-4,5-diphenyl imidazole (**1**). Yield 81%; colorless solid, mp 98−100 °C; IR (KBr) ν_{max}: 3448, 2916, 2845, 1597, 1588, 1495, 1465, 1394, 1250 cm^{-1}; ^1H NMR (300 MHz, $CDCl_3$): δ 782 (d, *J* = 7.5 Hz, 2H), 7.49 (br s, 4H), 7.28 (m, 6H), 7.04 (br s, 1H), 6.87 (d, *J* = 7.8 Hz, 2H), 3.92 (br s, 2H), 1.76 (t, *J* = 6.6 Hz, 2H), 1.27 (br s, 30H), 0.89 (t, *J* = 6.6 Hz, 3H); ^{13}C

DOI: 10.1021/acs.langmuir.7b01750
Langmuir 2017, 33, 8383−8394

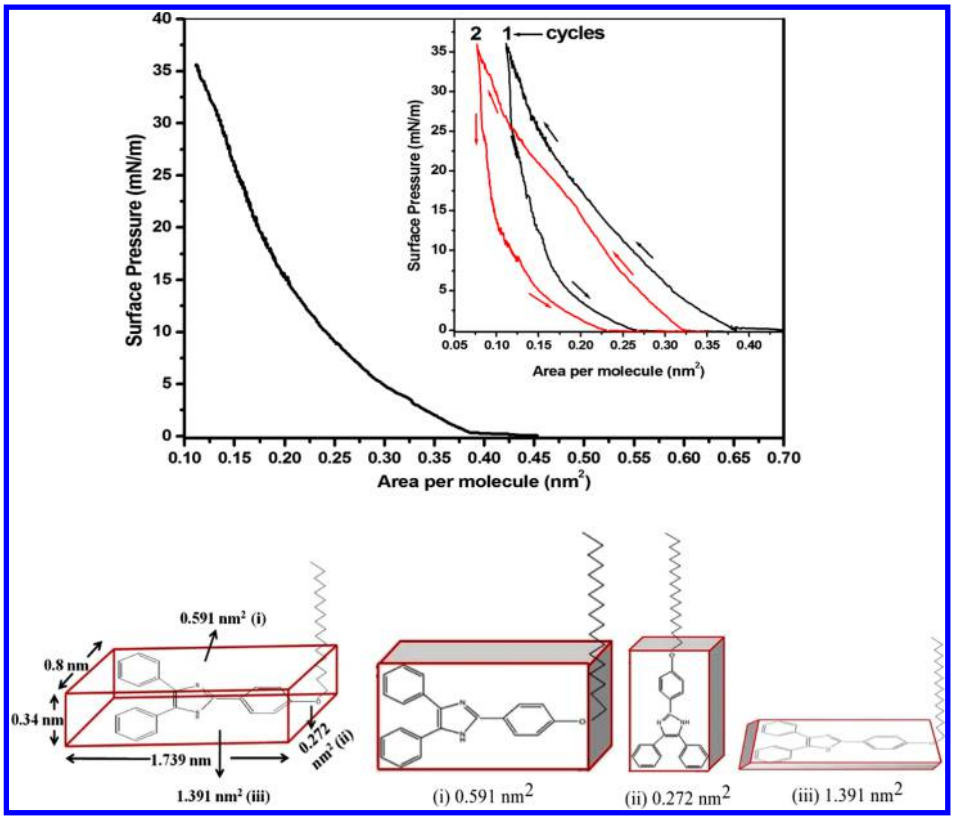

Figure 2. Surface pressure (π) vs area per molecule (A) isotherm of **1**. The inset shows the hysteresis of **1**. **1** moiety considered as a cuboid box; (i–iii) three possible orientations of **1** at the air–water interface.

NMR (75 MHz, $CDCl_3$): δ 159.9, 146,2, 132.5, 129.8, 128.5, 127.9, 127.4, 127.0, 121.9, 114.8, 68.1, 31.9, 29.7, 29.6, 29.4, 29.3, 29.2, 26.0, 22.7, 14.1; HRMS requires for $C_{39}H_{53}N_2O$ ($M + H^+$) 564.4157; found, 565.4159.

Synthesis of 1-Benzyl-2-(4-*O*-octadecyloxyphenyl)-4,5-diphenyl Imidazole (2). To a stirred mixture of 2-(4-*O*-octadecyloxyphenyl)-4,5-diphenyl imidazole (**1**, 1 mmol), anhydrous K_2CO_3 (2 mmol) in dry DMF (5 mL) and benzyl bromide (1.25 mmol) were added at 60 °C and was continued until the disappearance of the starting materials (~4 h). After completion of the reaction (TLC), the mixture was filtered and washed with ethyl acetate (25 mL). The combined organic layer was extracted with water (25 mL), washed with water (3 × 20 mL), dried over Na_2SO_4, and concentrated under reduced pressure. The crude product was purified by column chromatography using 2–5% ethyl acetate–hexane to afford the desired product. Yield 89%, white powder, mp 90 °C; IR (KBr) ν_{max}: 3020, 2941, 2856, 1597, 1467, 1369, 1270 cm^{-1}; ^1H NMR (300 MHz, $CDCl_3$): δ 7.71 (m, 1H), 7.55 (m, 4H), 7.34–7.13 (m, 10H), 6.90 (d, J = 9.0 Hz, 2H), 6.80 (m, 2H), 5.08 (s, 2H), 3.96 (t, J = 6.6 Hz, 2H), 1.80–1.67 (m, 4H), 1.48–1.40 (m, 2H), 1.25 (s, 26H), 0.88 (t, J = 6.6 Hz, 3H); ^{13}C NMR (75 MHz, $CDCl_3$): δ 159.7, 137.6, 131.1, 130.9, 130.4, 129.7, 128.8, 128.7, 128.5, 128.0, 127.3, 126.8, 126.3, 126.0, 114.6, 68.1, 48.2, 31.9, 30.55, 29.7, 29.6, 29.5, 29.4, 29.3, 29.2, 26.0, 22.7, 19.2, 14.1; HRMS requires for $C_{46}H_{59}N_2O$ ($M + H^+$) 564.4627; found, 655.4627.

Instruments. A commercially available LB film deposition instrument (Apex 2000C, Apex Instruments Co., India) was used for surface pressure–area isotherm measurements as well as for monolayer and multilayer film preparation. The AFM images of the monolayer films were taken by a commercial Innova AFM system (Bruker AXS Pte Ltd.) by using silicon cantilevers with a sharp, high apex ratio tip (Veeco Instruments). The AFM images presented here were obtained in the intermittent-contact ("tapping") mode. UV–vis absorption and fluorescence spectra of pure solutions as well as LB films were recorded by using an absorption spectrophotometer (PerkinElmer, Lambda 25) and a fluorescence spectrophotometer (PerkinElmer, LS 55), respectively. The attenuated total reflection (ATR)-FTIR spectra of the LB films deposited onto a ZnSe single-crystal were recorded using an FTIR spectrophotometer (PerkinElmer, model no. Spectrum 100, USA). BAM images were taken by using a commercial BAM system (Accurion nanofilm ep4-bam, serial no. 1601EP4030) equipped with a 30 mW laser emitting p-polarized light at 532 nm wavelength, which was reflected off the air–water interface at the Brewster angle (53.1°). XRD (Bruker D8 advance) data were obtained using monochromatic copper K_α radiation (wavelength 1.54 Å) and 2θ step of 0.02°. The current–voltage (I–V) characteristics were measured using a Keithley 2401 source meter.

Procedures. To measure the isotherms and for film preparation, 120 microliters of chloroform solution (0.5 mg/mL) of **1** was spread with a microsyringe onto the subphase of pure Milli-Q water (18.2 MΩ cm) at room temperature. After complete evaporation of the volatile solvent, the barrier was compressed at a rate of 5 mm/min to record the surface pressure–area per molecule isotherm. The surface pressure (π) versus average area available for one molecule (A) was measured by a Wilhelmy plate arrangement.[36] Smooth fluorescence grade quartz plates (for spectroscopy) and Si-wafers (for AFM studies) were used as the solid substrate. This was followed by the Y-type deposition at a particular surface pressure to transfer Langmuir films at a deposition speed of 5 mm/min. For AFM measurements, both single-layer and multilayer films were deposited. The transfer ratio was estimated by calculating the ratio of decrease in the subphase area to the actual area on the substrate coated by the layer and was found to be 0.98 ± 0.02. For the I–V characteristic study, freshly cleaned indium tin oxide (ITO)-coated glass plates were used as the solid substrate, and 60-layer LB films of **1** were deposited onto ITO-coated glass substrates at 10 mN/m surface pressure. Here, the ITO-coated glass substrate serves as the anode and a gold tip, softly touching the surface of the thin film, acts as the cathode, giving an active area of 1 mm^2 for measurement. The solutions were churned up for almost 10 h before the preparation of the films, and the as-prepared LB films were dried for more than 10 h before characterization. During the experiment, the samples were not allowed to be irradiated by any

DOI: 10.1021/acs.langmuir.7b01750
Langmuir 2017, 33, 8383–8394

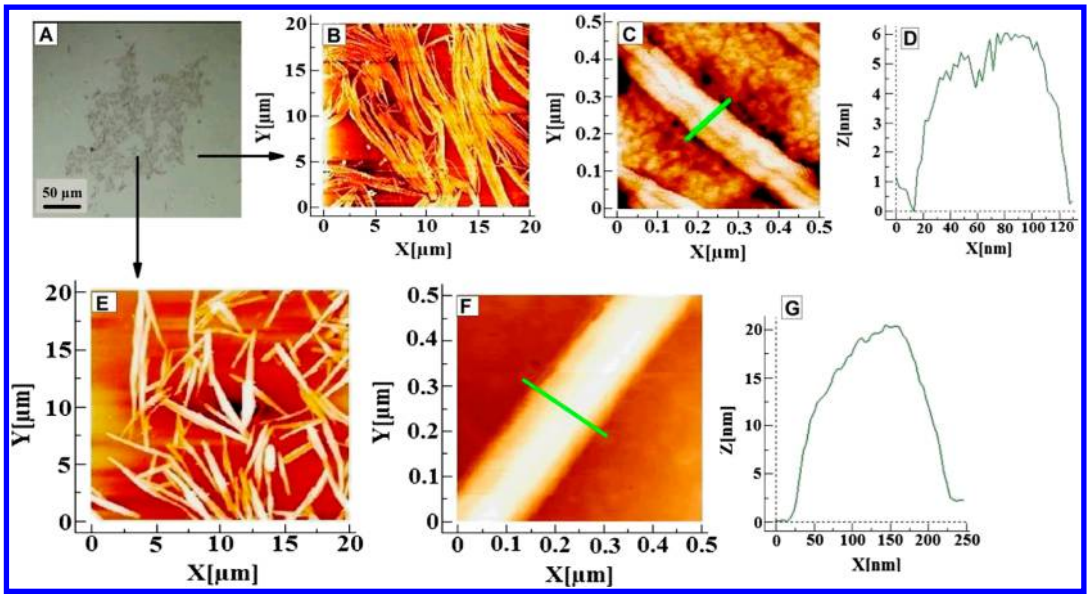

Figure 3. (A) Optical image; AFM images of the one-layer LB film of **1** at 5 mN/m (B) on optically blank space, (C) zoomed image, (D) analysis spectra of a single nanowire, (E) on optically shown structures, (F) zoomed image, and (G) analysis spectra of a single nanorod.

light and were always kept at room temperature. The $I-V$ curves were recorded by applying a sweeping voltage between 0 and 3 V at a voltage scan rate of 2.5 mV/s.

EXPERIMENTAL RESULTS

Surface Pressure–Molecular Area Isotherm. To study the monolayer forming behavior of **1**, surface pressure–area ($\pi-A$) isotherms of **1** at the air–water interface were recorded using the LB technique. Figure 2 shows the $\pi-A$ isotherm of **1** at the air–water interface. The isotherm was repeated several times and almost reproducible results were obtained. The curve presented here is the average of three independent measurements. The isotherm shows the onset of surface pressure at a molecular area of 0.43 nm^2/molecule (lift-off area) with the gaseous phase extending up to 0.32 mN/m (corresponding area per molecule = 0.37 nm^2). Then, the surface pressure rises smoothly up to 35.5 mN/m. No clear phase change between the liquid and condensed states is observed. Also, any sharp collapse at the end of the $\pi-A$ isotherm is not visible, indicating the formation of domains/multilayer instead of an ideal monolayer.[47] To have more insight into the system, an understanding about the possible molecular orientation of **1** at the air–water interface is necessary. On the basis of molecular modeling (CPK model) considering the **1** moiety as the cuboid box (Figure 2), the dimensions are estimated as 1.739 nm × 0.8 nm × 0.34 nm. These dimensions lead to three cross-sectional areas 1.391, 0.591, and 0.272 nm^2 (Figure 2i–iii). Our observed value of limiting molecular area was 0.25 nm^2, obtained from the extrapolation of the linear part of the isotherm to zero surface pressure. Though the value of the limiting molecular area is very close to 0.272 nm^2, for the vertical orientation (Figure 2ii), such a conformation is almost unlikely because of the absence of any polar group on the molecular backbone at the bottom for this orientation. The other two possible orientations of the molecule at the air–water interface are also not possible because of the large difference in their cross-sectional areas from the observed limiting molecular area of **1**. These facts do not support the formation of a monolayer at the air–water interface. Such results may occur either from the stacking of multilayers or from the formation of high-level supramolecular structures.[55,56] This may be due to the strong interaction between molecules in the assembly. The interaction includes the hydrogen bonding between the N–H groups, hydrophobic interaction between the alkyl chains, and $\pi-\pi$ interaction between the **1** molecules.

To have more information about the floating film at the air–water interface, successive compression–expansion cycles were also performed during the isotherm measurement. The inset of Figure 2 shows the resulting isotherm of two successive compression and decompression experiments. The result showed completely irreversible behavior with a marked shift toward the lower area per molecular region. This result supports the fact that molecule **1** did not form a stable monolayer at the air–water interface rather formed stacking of multilayers or high-level supramolecular structures.[57] It has been assumed that the origin of hysteresis observed in the compression–expansion experiment for the Langmuir film is associated with the manifestation of strong intermolecular interactions via $\pi-\pi$ interactions between the benzene ring and/or hydrogen bonding between the N–H group, resulting in the formation of aggregates/stacks at the air–water interface.[57,58]

To have the visual information, the floating film at the air–water interface was investigated using BAM. The BAM images were taken at various stages during the pressure–area isotherm measurement. All images clearly show that a uniform monolayer did not form at the air–water interface rather definite rodlike structures were formed at the air–water interface, although the size and packing change at different stages of the isotherm. Representative images are shown in Figure S1 of the Supporting Information.

An investigation of the floating behavior of molecule **1** at the air–water interface suggested that molecule **1** did not form a true monolayer at the air–water interface rather formed a multilayer or aggregates. To confirm whether there was free space available at the air–water interface just after spreading, we measured the $\pi-A$ isotherms by varying the concentration as well as the amount of the spread solution (Supporting Information, Figure S2). This also helped to start the isotherm with higher initial area per molecule. However, interestingly all isotherms were found to be almost similar except in certain cases where because of low concentration, surface pressure did not increase much. These results confirmed that the observed multilayer or aggregates of molecule **1** at the air–water interface was not due to very high concentration of the spread solution. Rather, the observed stacking/multilayer formation at the air–water interface was due to different kinds of interactions among the molecules at the air–water interface. Our later investigations revealed the nature of such interactions.

Morphology of the Transferred Films. Pressure–area isotherm of **1** was an indication that **1** did not form an ideal monolayer at the air–water interface rather indicated toward the formation of supramolecular nanostructures. To get an insight into the morphology of the possible nanostructures formed at the air–water interface, the floating Langmuir monolayer of **1** was transferred onto a solid substrate under various conditions for further characterization.

DOI: 10.1021/acs.langmuir.7b01750
Langmuir 2017, 33, 8383–8394

Table 1. Width of Nanowires and Nanorods at Different Pressures in the One-Layer LB Film of 1

	width of nanostructures at pressure			
structures	5 mN/m	10 mN/m	15 mN/m	20 mN/m
nanowires	110 nm	200 nm	140−150 nm	75−100 nm
nanorods	200−250 nm	500 nm	700 nm	250−300 nm

Initially for AFM characterization, the monolayer of **1** was deposited onto a clean smooth silicon substrate at 5 mN/m surface pressure following a vertical (Y-type) deposition mode. Before measuring the AFM image, the film was observed through an optical microscope. Interestingly, optical microscope images (Figure 3A) suggest two different morphologies: (i) few parts with accumulated structures and (ii) parts with optically blank areas. During AFM imaging, specific attention was given to study these two different regions.

The AFM images measured on the optically blank region exhibit wirelike nano-structures throughout the film (Figure 3B). The lengths of the nanowires were several micrometers long. The diameter and height of the individual nanowires were approximately 100−110 and 6−8 nm, respectively (Figure 3C,D).

On the other hand, the AFM images measured on the area of the **1** LB film, showing structures (optically visible), revealed assemblies of nanorod-like structures having a length of 8−10 μm (Figure 3E). The width and height of the rods were approximately 200−250 and 20−22 nm, respectively (Figure 3F,G). The AFM images of the nanowires and nanorods with different scan areas for the same **1** in the LB film are shown in Figures S3 and S4, respectively, in the Supporting Information.

Pressure Effect. To check the effect of surface pressure on the morphology of nanostructured LB films of **1**, the floating films was transferred onto a silicon wafer substrate at different surface pressures viz. 10, 15, and 20 mN/m. Under an optical microscope, all films showed regions with two different morphologies: blank surface as well as accumulated regions as seen in the film deposited at 5 mN/m surface pressure. The AFM images of all films showed either nanowire- or nanorod-like structures for two different regions in the films. However, variation in the size and shape/organization of nanostructures in the films was observed depending on the surface pressure of the deposition (Table 1).

In the case of the nanowire, although the height remained almost the same, the width changes with the surface pressure, and maximum width was observed for the film deposited at 10 mN/m (Figure 4A,B and Table 1). On the other hand, in the case of the nanorod, both the width as well as height changed with the surface pressure. Initially, both the width and height increased with surface pressure and then decreased. Maximum height and width were observed for the film deposited at 15 mN/m surface pressure (Figure 4C,D and Table 1). Several other AFM images for different pressures in one-layer **1** LB film are shown in the Supporting Information (Figure S5).

Aging Effect. Supramolecular organic nanostructures play a key role toward organic electronics through improvement of semiconducting, conducting, memory, storage, and display performances. It has been observed that **1** formed organized nanowire- and nanorod-like structures in LB films. An understanding of the time-dependent changes in such nanostructures is very important for their application. Accordingly, the morphology of **1** LB films with passage of time was studied using AFM. To do that, one-layer LB film of **1** was deposited on a smooth clean silicon substrate, and the morphology of the film surface was studied using AFM at regular intervals for several days.

Our observation revealed interesting results. Although the width and thickness of the individual nanowire and nanorod remained almost unaltered with the passage of time, the alignment and organization of the nanorod and nanowire changed in the LB films with the passage of time. Initially, the organization of the nanowires in the LB films was arbitrary with hardly any definite directionality. However, with passage of time, the nanowires came close to each other and became straight with respect to each other in the LB films (Figure 5A,B). As a whole, the organization of the nanowire changed in the LB films. Such changes in the organization occurred up to 5 days from the day of preparation of the films. However, after 5 days, almost no further changes in the film surface morphology were observed, indicating

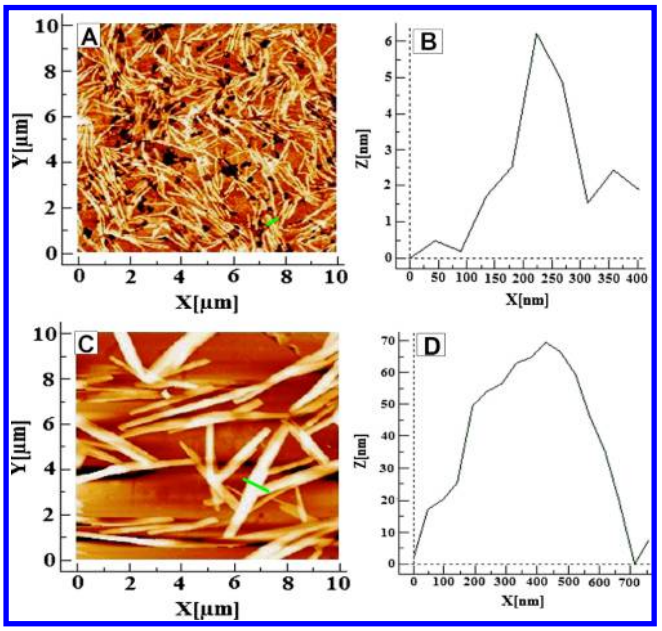

Figure 4. (A) AFM images of nanowires in the one-layer LB film of the **1** molecule at 10 mN/m. (B) Analysis spectra of nanowires. (C) Nanorods in the one-layer LB film of **1** at 15 mN/m. (D) Analysis spectra of nanorods.

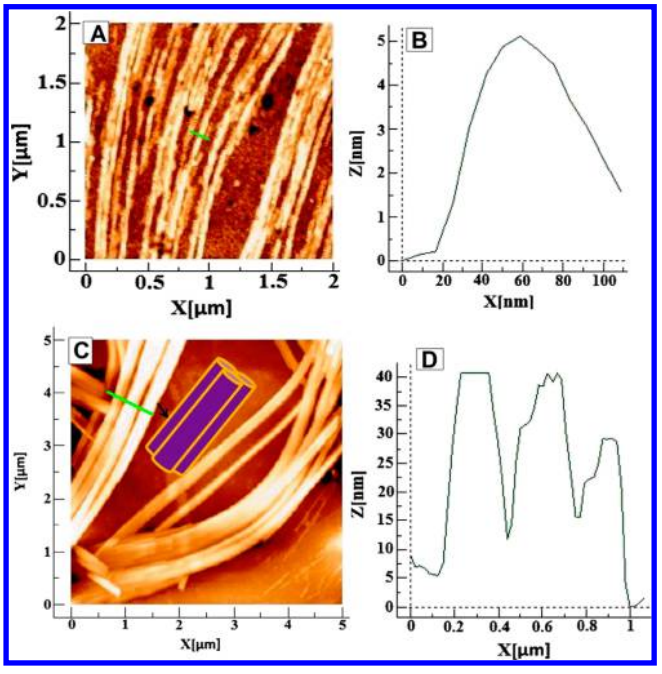

Figure 5. (A) AFM images of the nanowire after 5 days in the one-layer LB film of the **1** molecule at 5 mN/m. (B) Analysis spectra of the nanowire. (C) Nanorods after 5 days. (D) Analysis spectra of the nanorod.

DOI: 10.1021/acs.langmuir.7b01750
Langmuir 2017, 33, 8383−8394

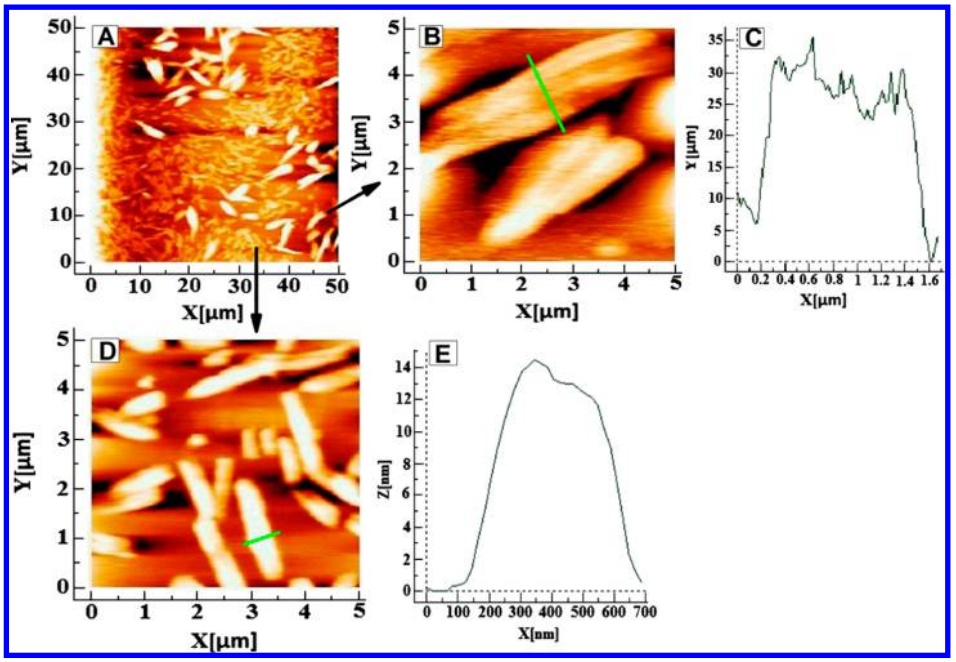

Figure 6. AFM image of the 10-layer LB film of **1** at 5 mN/m.

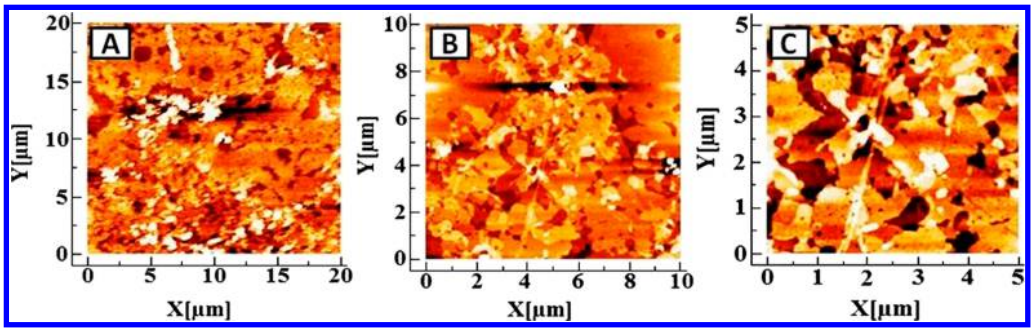

Figure 7. AFM image of **2** in the one-layer LB film at 5 mN/m with different scan areas—(A) 20 × 20 μm^2, (B) 10 × 10 μm^2, and (C) 5 × 5 μm^2.

attainment of maximum stable configuration of **1** nanowire in the LB films.

On the other hand, in the case of nanorods, with passage of time, the nanorods came close to each other and formed bundles of several rods in the LB films (Figure 5C,D). Here also, the change in the film morphology occurred up to 5 days of film formation, and maximum stable configuration of **1** nanorod occurred within 5 days of preparation of LB films. Several other AFM images showing the effect of aging day by day in the nanorods and nanowires are shown in Figures S6 and S7, respectively, in the Supporting Information.

Layer Effect. Compound **1** formed supramolecular structures in the one-layer LB film. To check the effect of multilayer deposition of the nanostructures of **1** onto LB films, 10-layer LB films of floating **1** films were deposited onto a silicon substrate and studied using AFM. Corresponding AFM images (Figure 6A) showed interesting results with modified nanostructures.

Here, the nanowires (formed in one-layer LB films) are broken in length, and several broken nanowires are bundled together to form nanorod-like structures (Figure 6D). The width is 4−5 times and the height is almost double (Figure 6E) compared to the nanowires that formed in one-layer LB films (Figure 3D). However, the length was within the 1−2 μm range.

On the other hand, in the case of multilayer films, the nanorods are attached with each other. Here, four to five nanorods join together to form bigger bundles in the multilayer LB films (Figure 6B,C).

DISCUSSION

Generally, the amphiphilic molecules can exhibit relatively strong hydrophobicity as they have a quite long alkyl chain and their head groups contain aromatic rings. When these amphiphilic molecules are spread onto the air−water interface, some of them tend to assemble into multilayer films or more complicated nanostructures instead of forming an ideal monolayer.[45] It has already been explained that such nanostructures at the air−water interface may be due to various noncovalent bonds such as the hydrogen bond, $\pi-\pi$ stacking of the π-conjugated end groups, electrostatic interaction, hydrophobic interaction of the hydrophobic spacer, and so forth.[59]

In the present case, the absence of a sharp collapse and the observed lower value of the limiting area per molecule in the surface pressure versus area per molecule isotherm of **1** suggested that imidazole derivative **1** did not form an ideal monolayer at the air−water interface. It has been reported that 2-(heptadecyl)naphtha[2,3]imidazole (NplmC17) also did not form an ideal monolayer and showed a too small limiting area per molecule.[54] The observed small molecular area suggested the strong interaction between the **1** molecules within the assemblies, which may include the hydrogen bonding of the N−H group, hydrophobic interaction between the alkyl chain, and also $\pi-\pi$ interaction. These features of the isotherm are an

DOI: 10.1021/acs.langmuir.7b01750
Langmuir 2017, 33, 8383−8394

indication of the formation of supramolecular nanostructures of **1** at the air−water interface.[60] Liu et al. observed a small area per molecule when cinnamoyl-terminated bolaamphiphiles formed aggregated nanostructures at the air−water interface.[45,59] Azobenzene derivative also formed surface pressure-driven supramolecular structures showing a small molecular area at the air−water interface.[47]

The AFM image of **1** LB film showed the formation of nanowires and nanorods in a one-layer LB film. We assume that the intermolecular H-bond between N−H of one imidazole ring and =N of another neighboring **1** molecule may play a crucial role in the formation of such nanostructures in the LB films. To check this possibility, we synthesized a new molecule (compound **2**) having an almost similar structure to that of **1**. The only difference is that the N−H group present in **1** was replaced by a benzyl group in **2**. After that, we prepared a one-layer LB film of **2** onto a silicon wafer and investigated using AFM. The AFM analysis revealed that the **2** molecule did not form nanostructures in LB films. AFM images for **2** in the LB monolayer are shown in Figure 7. The interesting thing is that because of the absence of the N−H group in the molecular structure of **2**, no H-bonding formed at the air−water interface. Accordingly, no nanostructures were observed. This justified our assumption that the H-bonding between the N−H and =N groups of the neighboring **1** molecule in case of **1** assembly at the air−water interface and in the LB film plays a vital role in the formation of supramolecular nanostructures in one-layer LB films. Liu et al. also reported that imidazole derivatives formed different kinds of nanostructures because of H-bonding between the N−H group present in the molecular structure and J-aggregate formation in the LB films.[48] There are several reports where it has been explained that because of H-bonding, different nanostructures were observed in the LB films under various conditions.[44,45,59,61]

FTIR spectroscopy is a powerful tool to have an idea about vibrational changes during the molecular interaction. This method is particularly very useful for investigating the system where a reaction has occurred. We also measured the FTIR spectra of molecule **1** in the LB film as well as in the KBr pellet. Important band positions are listed in Table 2, and the corresponding spectra are shown in Figure 8.

Table 2. Important Band Positions in the FTIR Spectra of 1 in the KBr pellet and in LB Films

band positions (cm^{-1}) (compound **1**)			
in KBr pellet	in LB film	band assignment	band shift (cm^{-1})
3448	3415	N−H stretching vibration	33
2919	2915	CH_2 asymmetric vibration	4
2849	2840	CH_2 symmetric vibration	9
1465	1477	CH_2 scissoring vibration	12
1250	1241	CH_2 wagging vibration	9

Indication about the H-bonding has been confirmed from the observed difference in the position as well as intensity of the N−H stretching vibration between the FTIR spectra in the LB film and in the KBr pellet. Nitrogen in the imidazole molecule can form H-bonds with hydrogen in the N−H group of the neighboring molecule.[48] On the other hand, the bands due to the vibration of CH_2 of the alkyl chain are largely affected in the LB film compared to that in KBr. This clearly indicated the change in orientation of the alkyl chain in LB films.[45,49−51,59] It

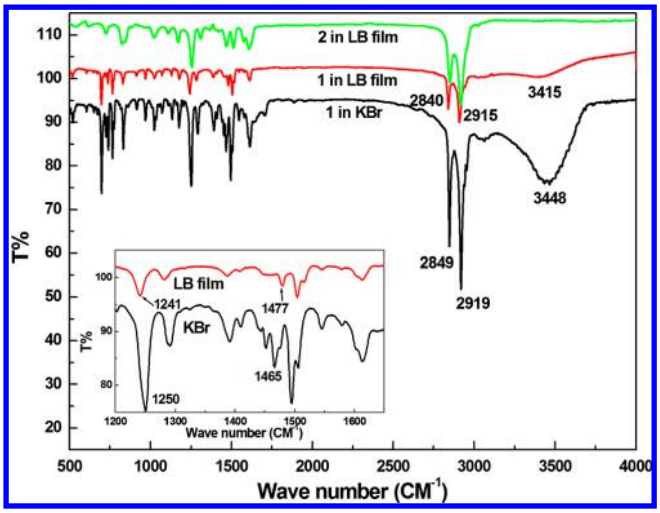

Figure 8. FTIR spectra of **1** in the KBr pellet (black) and in the 10-layer LB film (red) along with the FTIR spectra of **2** in the LB film (green) deposited at 5 mN/m. The inset shows the magnified FTIR spectra of **1** in the wavelength range of 1200−1700 cm^{-1} for better comparison.

has been observed that compound **2** did not form any supramolecular nanostructures like molecule **1** in LB films. It has been assumed that because of the absence of N−H group, no H-bond formed in case of compound **2** in LB films. Accordingly, no nanostructures were observed. To justify this hypothesis, FTIR spectra of **2** were also measured and are presented in Figure 8. The absence of a band system within 3100−4000 cm^{-1} clearly confirmed that no H-bonding was formed in the LB film of molecule **2**.

It has been reported that $\pi-\pi$ stacking in J-aggregates as well as other aggregates, for example H-aggregate, plays an important role toward the formation of different kinds of supramolecular structures in LB films.[46,48] To check the possible aggregation nature of **1** in the LB film, we have recorded the UV−vis absorption and fluorescence spectra of **1** in solution and in LB films. The solution spectrum of **1** possessed a prominent intense 0−0 band at 303 nm. For LB films of **1**, an overall broadened absorption spectrum appeared at 321 nm along with a red shift of 18 nm with respect to pure **1** in solution. The broadening of the absorption spectrum along with the red shift may be due to the formation of J-aggregates in LB films. The corresponding absorption spectra of **1** in solution and in the LB film are given in the Supporting Information (Figure S8). The fluorescence spectrum of **1** in solution showed a prominent peak at 396 nm, whereas in the case of the LB film, the same has been shifted to 387 nm. Excitation spectra with monitoring wavelength fixed at the emission maximum for both the solution and LB film have also been recorded. The observed difference in the excitation spectra for the solution and film with respect to the band position and broadening also confirmed the possible aggregation of molecule **1** in LB films. The corresponding fluorescence spectra and excitation spectra are shown in Figure S9 of the Supporting Information. Therefore in the present case, in addition to H-bonding, J-aggregate also played a crucial role toward the formation of nanostructures in LB films.

On the basis of the experimental results of AFM and spectroscopic investigations, we tried to propose a model (Scheme 1) for the formation of nanowires and nanorods at the air−water interface and in LB films of **1**. There exist few reports

DOI: 10.1021/acs.langmuir.7b01750
Langmuir 2017, 33, 8383−8394

Scheme 1. Formation Mechanism of Surface Pressure-Driven Supramolecular Nanostructures

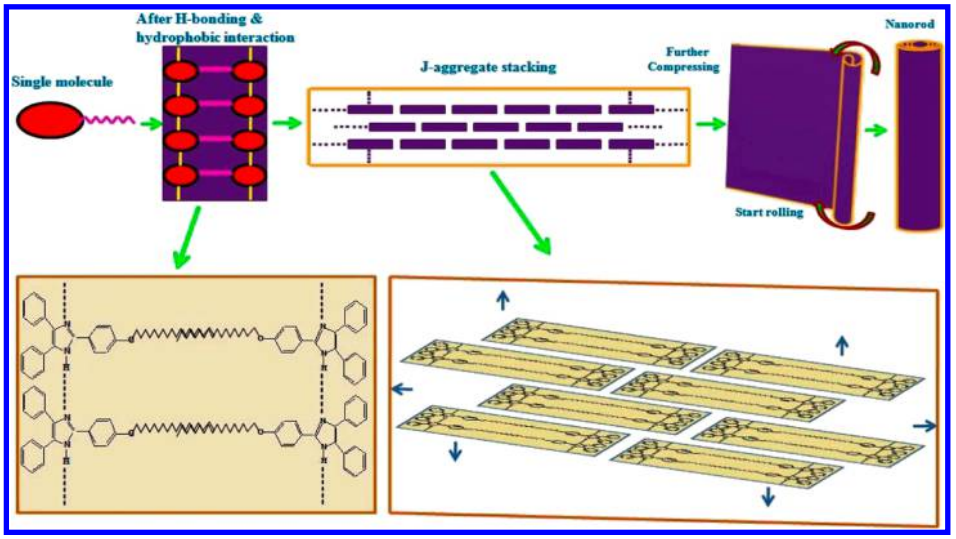

showing the formation of such nanowire- and nanorod-like assembly of organic amphiphiles.[45−48,59] They also proposed models for the formation of such a nanoassembly.[45−47] In few cases, surface pressure-driven rolling of the organized layer at the air−water interface has been suggested.[45−47] In the present case, microscopic results revealed the formation of nanowire- and nanorod-like structures. Also, H-bonding between the N−H groups of **1** occurred at the air−water interface. On the other hand, the absorption spectroscopic study suggested the possibility of J-aggregate formation. In J-aggregates, molecules are stacked together with head-to-tail arrangements.[62,63]

To have an idea about molecular organization in the aggregates, we performed the XRD study for a 10-layer LB film of **1**. The corresponding spectra is shown in the Supporting Information (Figure S10). The XRD spectra show prominent sharp peaks with 2θ = 22.03, 38.28, 44.43, 64.91, 68.86, and 79.18°, indicating the formation of an ordered crystalline structure in the LB films. A similar feature in the XRD spectra for other imidazole derivatives has also been reported.[64,65] The calculated layer distance was found to be on the order of 0.4 nm corresponding to 2θ = 22.03° using Bragg's equation. This distance is assigned to the distance between two adjacent **1** molecules in the longitudinal direction.[66] Considering the dimensions of the present molecule as 1.739 nm × 0.8 nm × 0.34 nm, the observed distance is consistent with the typical distance for effective $\pi-\pi$ stacking between the aromatic molecules. This suggests that molecule **1** remained flat horizontally in the multilayer.

Therefore, it might be possible that because of H-bonding, several **1** molecules might connect together horizontally at the air−water interface and stack together to form a large nanosheet-like arrangement at the air−water interface. Also, there exists a strong hydrophobic interaction due to the presence of a long alkyl chain of the **1** molecule.[59] Owing to the strong hydrophobicity upon compression, the nanosheet/layer may tend to roll up into a nanowire or nanorod.[46] To check the effect of compression on the formation of **1** nanostructure, we deposited a film of **1** onto a Si-substrate at zero surface pressure. The AFM image of the corresponding film did not show any nanowire/nanorod-like structures (Figure S11) as seen in the film deposited at definite pressures. Therefore, it can be said that in the present case, the **1** molecule formed a nanosheet-like structure at the air−water interface after spreading because of H-bonding and J-aggregate formation. Upon compression, this nanosheet rolled up to form a nanowire/nanorod-like structure. However, in the present case, two types of nanostructures/nanowires and nanorods were formed. This may be due to a different order of stacking during aggregation at the air−water interface and also the extent of rolling during compression.

We have also checked the AFM images of the drop-cast as well as spin-coated films prepared using the same solution (Figure S12). Interestingly, no such nanostructures were observed in the corresponding images as seen in the LB films. This also indicates that the LB technique has a specific role in the formation of observed supramolecular nanostructures (nanowire/nanorod) in thin films.

It has been observed that the width and height of the nanostructures changed with an increase in the surface pressure of lifting. This may be due to a change in the extent of stacking of the **1** molecule in the aggregate before the rolling occurred with surface pressure during compression. On the other hand, with aging, organization of **1** nanowires changed. They seemed to be straightened with aging and became stable after few days. Also, several nanorods came close to each other and formed bundles with aging. There might exist some interaction between the corresponding nanostructures within the film, resulting in modification of the alignment as well as arrangement in the films. Absorption spectroscopic study (Figure S8) of the **1** LB film with aging also showed some changes of the aggregation band, indicating a change in the aggregation nature in the LB films with time. However, after few days, the film attained stable condition. It is relevant to mention in this context that a change in the aggregation nature in the LB film has already been reported by several authors.[67,68] It has been explained as due to the molecular movement that occurred within the LB film resulting in a change in aggregation.[69,70]

■ SWITCHING BEHAVIOR

Organic nanostructures assembled onto LB films are very promising with respect to their possible application in molecular electronic devices.[71] In the present study, imidazole derivative **1** formed nanostructures when organized onto LB

DOI: 10.1021/acs.langmuir.7b01750
Langmuir 2017, 33, 8383−8394

films. Imidazole derivatives can readily form a donor−acceptor system when tailored with various aromatic groups and possess various attractive properties in terms of conductivity, luminescence, and color tunability.[72−74] We do believe that nanostructures of **1** in LB films may be an interesting input toward the component of future organic electronic devices.

Here, we have investigated the electrical switching behavior of **1** assembled onto LB films. In a switching device, two conducting states (low and high) are observed at the same applied voltage.[75] This type of bistable organic switching behavior is promising for next-generation information storage and future optoelectronic devices.[76,77] We expected the switching behavior using **1** because of the presence of the electron donor−acceptor group in the **1** molecule (Figure 1).

A typical *I*−*V* characteristic curve of **1** in the LB film is shown in Figure 9. As a reference, the *I*−*V* characteristic of

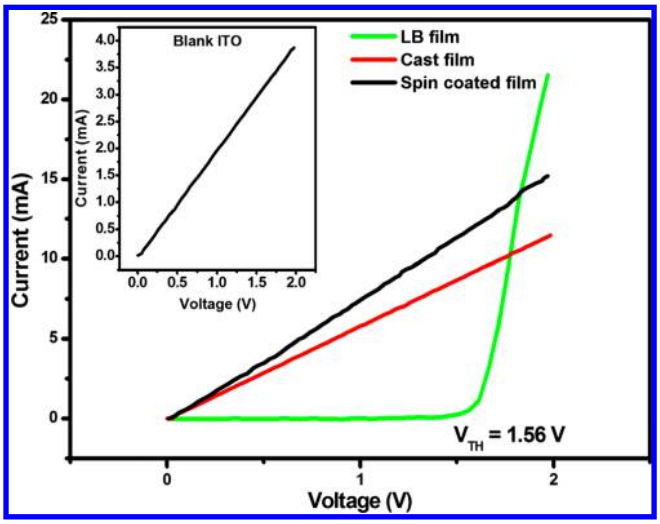

Figure 9. *I*−*V* characteristic of **1** in the 60-layer LB, spin-coated, and drop-cast films. The inset shows the *I*−*V* characteristic of blank ITO.

blank ITO has also been presented in Figure 9 (inset) for comparison. From the figure, it can be observed that pure ITO showed linear Ohmic behavior as expected.[9,78,79] On the other hand, clear switching behavior can be observed for molecule **1** in the LB film. During scanning at lower voltage, the film exhibited its low conducting state (OFF state) initially. When the voltage approached the so-called threshold voltage (about 1.5 V), the current increased rapidly, showing its high conducting state (ON state).

To check the role of the LB technique on such observed switching behavior, we also prepared drop-cast as well as spin-coated films of **1** on the ITO-coated glass substrate and checked their *I*−*V* characteristics. However, the observed results (Figure 9) did not show any switching phenomenon, rather showed linear Ohmic behavior. This clearly indicates the role of the LB technique toward the electrical switching behavior of molecule **1**.

Because of the presence of the electron donor−acceptor system in the **1** molecule, electrical charges are particularly transferred from the donor to the acceptor moiety in LB films.[80,81] However, in the case of drop-cast/spin-coated films, the charge transfer may be disturbed because of the bulk nature of the films. A sharp increase in conductivity occurred after the charge had been transferred. Because of the presence of the donor−acceptor group, Cu−tetracyanoquinodimethane (TCNQ) showed resistive switching behaviur.[82] Using Raman spectroscopy, it has been confirmed that anions were changed into neutral components during the charge transfer process.[83] Chu et al. also reported bistable switching phenomenon using [6,6]-phenyl-C_{61}-butyric acid methyl ester (PCBM) and tetrathiofulvalene (TTF) because of charge transfer in the donor−acceptor moiety.[80] It has also been observed that the threshold voltage changed with the aging of **1** in LB films. In the present case, the observed switching behavior was due to the charge transfer between the donor−acceptor sites of compound **1**. However, further investigations are required to know the exact mechanism of switching behavior of compound **1** in LB films. Also, we do believe that an identical study of optical and electrical behaviors of compound **1** in thin films may give some valuable information toward its practical application in optoelectronic devices. Investigations are going on in this line in our lab.

CONCLUSIONS

In summary, we have designed a 2,4,5-triaryl imidazole derivative and studied its assembly behavior at the air−water interface and in thin films by the LB technique. This molecule may be an interesting candidate for organic electronics because of the presence of oxygen atom in position 4, which can act as the electron donor, and the ═N group or other phenyl aryls at C-4 or 5, which can act as the electron acceptor in **1**, to generate a dipolar push−pull system (D−π−A) that assures intramolecular charge transfer. Also, the long alkyl chain and N−H of the imidazole core may help to form supramolecular architecture through the hydrophobic−hydrophobic interaction and hydrogen bonding. The absence of a sharp collapse and the observed lower value of limiting area per molecule in the pressure−area isotherm of **1** indicated the formation of domains/multilayer instead of an ideal monolayer. This was confirmed by hysteresis analysis and BAM measurement. AFM investigations successfully demonstrated the formation of supramolecular nanowire- as well as nanorod-like structures in LB films. The height and width of the individual nanowires were nearly 6−8 and 100−110 nm, respectively. For nanorods, the height and width were nearly 20−25 and 200−250 nm, respectively. We have found that the morphology of such nanostructures were strongly dependent on the surface pressure of deposition and layer number as well as on aging. The height of the nanowires remained almost same but the width changed with surface pressure, and maximum width was observed at a surface pressure of 10 mN/m. In case of nanorods, both the width as well as height changed with surface pressure, and maximum value (width 700 nm and height 70 nm) was observed for the film deposited at 15 mN/m surface pressure. Upon aging, the morphology of such nanostructures changed in LB films. With passage of time, the nanowires came closer to each other and became straight with respect to each other in the LB films. The nanorods also came closer to each other with the passage of time and formed bundles of several rods in the LB films. Such changes occurred within 5 days of film formation, and no further changes occurred afterward. In case of 10-layer LB films, the nanowires were broken in length, and several broken nanowires were bundled together to form a nanorod-like structure. On the other hand, four to five nanorods joined together to form bigger bundles in the multilayer LB films. FTIR spectra clearly indicated the formation of H-bonding and change in the orientation of the alkyl chain in the LB film of **1**. UV−vis and fluorescence spectra

DOI: 10.1021/acs.langmuir.7b01750
Langmuir 2017, 33, 8383−8394

revealed the formation of J-aggregate of **1** in LB films. The formation of an ordered crystalline structure in the LB films has been confirmed by XRD analysis. The calculated layer distance from XRD spectra was consistent with effective $\pi-\pi$ stacking between the aromatic molecules and suggested that molecule **1** remained flat horizontally in the multilayer.

Our overall investigation revealed that H-bonding between the N−H group of **1**, J-aggregate, as well as compression during film preparation play a vital role toward the formation of supramolecular nanostructures. A model has been proposed to have an idea about the formation mechanism for such nanostructures in LB films. *I*−*V* characteristics showed the electrical switching behavior of **1** in 60-layer LB films. Apart from memory applications, the use of such organic switching behavior in logic elements of integrated circuits is also feasible.

■ ASSOCIATED CONTENT

Supporting Information

The Supporting Information is available free of charge on the ACS Publications website at DOI: 10.1021/acs.langmuir.7b01750.

BAM images of **1** at the air−water interface; $\pi-A$ isotherms at different concentrations and spread volumes; AFM images for nanowires and nanorods of **1** in the LB monolayer lifted at 5 mN/m surface pressure having different scan areas; AFM images of **1** in the LB monolayer deposited at different surface pressures; AFM images of **1** in the LB film measured with passage of time to have an idea about ageing; UV−vis spectra, fluorescence spectra, and XRD spectra of **1** in LB films; AFM images of **1** in the LB film deposited at 0 mN/m surface pressure; and AFM images of **1** for spin-coated and drop-cast films (PDF)

■ AUTHOR INFORMATION

Corresponding Author

*E-mail: sa_h153@hotmail.com, sahussain@tripurauniv.in. Phone: +919862804849, +91381 2375317. Fax: +913812374802.

ORCID

Syed Arshad Hussain: 0000-0002-3298-6260

Author Contributions

B.D., S.M., and S.A.H. designed the work. B.D., P.D., and S.C. performed all experiments and data analysis. S.M. and B.D. synthesized the material. S.A.H. and B.D. wrote the manuscript with input from D.B. and S.M.

Notes

The authors declare no competing financial interest.

■ ACKNOWLEDGMENTS

The authors are grateful to the DST, Government of India, for the financial support to carry out this research work through DST project ref EMR/2014/000234 and FIST DST project ref. SR/FST/PSI-191/2014. The authors are also grateful to the UGC, Government of India for the financial support to carry out this research work through financial assistance under UGC−SAP program 2016. One of the authors P.D. would like to acknowledge the DST, Government of India for providing financial support through INSPIRE fellowship.

■ REFERENCES

(1) Ahrens, M. J.; Fuller, M. J.; Wasielewski, M. R. Cyanated Perylene-3,4-dicarboximides and Perylene-3,4:9,10-bis-(dicarboximide): Facile Chromophoric Oxidants for Organic Photonics and Electronics. *Chem. Mater.* **2003**, *15*, 2684−2686.

(2) Jones, B. A.; Ahrens, M. J.; Yoon, M.-H.; Facchetti, A.; Marks, T. J.; Wasielewski, M. R. High-Mobility Air-Stable n-Type Semiconductors with Processing Versatility: Dicyanoperylene-3,4:9,10-bis(dicarboximides). *Angew. Chem., Int. Ed.* **2004**, *43*, 6363−6366.

(3) Zhan, X.; Tan, Z.; Domercq, B.; An, Z.; Zhang, X.; Barlow, S.; Li, Y.; Zhu, D.; Kippelen, B.; Marder, S. R. A High-Mobility Electron-Transport Polymer with Broad Absorption and Its Use in Field-Effect Transistors and All-Polymer Solar Cells. *J. Am. Chem. Soc.* **2007**, *129*, 7246−7247.

(4) Lindner, S. M.; Kaufmann, N.; Thelakkat, M. Nanostructured Semiconductor Block Copolymers: $\pi-\pi$ Stacking, Optical and Electrochemical Properties. *Org. Electron.* **2007**, *8*, 69−75.

(5) Jiménez, Á. J.; Spänig, F.; Rodríguez-Morgade, M. S.; Ohkubo, K.; Fukuzumi, S.; Guldi, D. M.; Torres, T. A Tightly Coupled Bis(zinc(II) phthalocyanine)−Perylenediimide Ensemble To Yield Long-Lived Radical Ion Pair States. *Org. Lett.* **2007**, *9*, 2481−2484.

(6) Chen, H. Z.; Ling, M. M.; Mo, X.; Shi, M. M.; Wang, M.; Bao, Z. Air Stable n-Channel Organic Semiconductors for Thin Film Transistors Based on Fluorinated Derivatives of Perylene Diimides. *Chem. Mater.* **2007**, *19*, 816−824.

(7) Belfield, K. D.; Bondar, M. V.; Hernandez, F. E.; Przhonska, O. V. Photophysical Characterization, Two-Photon Absorption and Optical Power Limiting of Two Fluorenylperylene Diimides. *J. Phys. Chem. C* **2008**, *112*, 5618−5622.

(8) Shirota, Y. Organic Materials for Electronic and Optoelectronic Devices. *J. Mater. Chem.* **2000**, *10*, 1−25.

(9) Forrest, S. R.; Thompson, M. E. Introduction: Organic Electronics and Optoelectronics. *Chem. Rev.* **2007**, *107*, 923−925.

(10) Miller, R. D.; Chandross, E. A. Introduction: Materials for Electronics. *Chem. Rev.* **2010**, *110*, 1−2.

(11) Louis, C.; Bazzi, R.; Marquette, C. A.; Bridot, J. L.; Roux, S.; Ledoux, G.; Mercier, B.; Blum, L.; Perriat, P.; Tillement, O. Nanosized Hybrid Particles with Double Luminescence for Biological Labeling. *Chem. Mater.* **2005**, *17*, 1673−1682.

(12) Morán, J. R.; Blázquez, M. T.; Muñiz, F. M.; Sáez, S.; Simón, L. M.; Alonso, A.; Raposo, C.; Lithgow, A.; Alcázar, V. Acridone Heterocycles as Fluorescent Sensors for Anions. *Heterocycles* **2006**, *69*, 73−81.

(13) Costa, S. P. G.; Oliveira, E.; Lodeiro, C.; Raposo, M. M. M. Synthesis, Characterization and Metal Ion Detection of Novel Fluoroionophores Based on Heterocyclic Substituted Alanines. *Sensors* **2007**, *7*, 2096−2114.

(14) Fang, Z.; Wang, S.; Zhao, L.; Xu, Z.; Ren, J.; Wang, X.; Yang, Q. A Novel Polymerizable Imidazole Derivative for Blue Light-Emitting Material. *Mater. Lett.* **2007**, *61*, 4803−4806.

(15) Sun, Y.-F.; Cui, Y.-P. The Synthesis, Structure and Spectroscopic Properties of Novel Oxazolone-, Pyrazolone- and Pyrazoline-Containing Heterocycle Chromophores. *Dyes Pigm.* **2009**, *81*, 27−34.

(16) Huang, S.; Li, Z.; Li, S.; Yin, J.; Liu, S. Imidazole-Based Dithienylethenes as a Selective Chemosensors for Iron(III) ions. *Dyes Pigm.* **2012**, *92*, 961−966.

(17) Yan, Y.-X.; Sun, Y.-H.; Tian, L.; Fan, H.-H.; Wang, H.-Z.; Wang, C.-K.; Tian, Y.-P.; Tao, X.-T.; Jiang, M.-H. Synthesis, Characterization and Optical Properties of a New Heterocycle-Based Chromophore. *Opt. Mater.* **2007**, *30*, 423−426.

(18) Yan, Y.-X.; Fan, H.-H.; Lam, C.-K.; Huang, H.; Wang, J.; Hu, S.; Wang, H.-Z.; Chen, X.-M. Synthesis, Structures, and Two-Photon Absorption Properties of Two New Heterocycle-Based Organic Chromophores. *Bull. Chem. Soc. Jpn.* **2006**, *79*, 1614−1619.

(19) Zhang, M.; Li, M.; Zhao, Q.; Li, F.; Zhang, D.; Zhang, J.; Yi, T.; Huang, C. Novel Y-Type Two-Photon Active Fluorophore: Synthesis and Application in Fluorescent Sensor for Cysteine and Homocysteine. *Tetrahedron Lett.* **2007**, *48*, 2329−2333.

DOI: 10.1021/acs.langmuir.7b01750
Langmuir 2017, 33, 8383−8394

(20) Kulhánek, J.; Bureš, F. Imidazole as a Parent π-Conjugated Backbone in Charge-Transfer Chromophores. *Beilstein J. Org. Chem.* **2012**, *8*, 25−49.
(21) Feng, K.; Hsu, F.-L.; Van Derveer, D.; Bota, K.; Bu, X. R. Tuning Fluorescence Properties of Imidazole Derivatives with Thiophene and Thiazole. *J. Photochem. Photobiol., A* **2004**, *165*, 223−228.
(22) Li, Z.; Lin, Y.; Xia, J.-L.; Zhang, H.; Fan, F.; Zeng, Q.; Feng, D.; Yin, J.; Liu, S. H. Synthesis of Novel Diarylethene Compounds Containing Two Imidazole Bridge Units and Tuning of Their Optical Properties. *Dyes Pigm.* **2011**, *90*, 245−252.
(23) Yuan, J.; Li, Z.; Hu, M.; Li, S.; Huang, S.; Yin, J.; Liu, S. H. Synthesis and Photochromic Properties of Imidazole-Based Diarylethenes. *Photochem. Photobiol. Sci.* **2011**, *10*, 587−591.
(24) Park, S.; Kwon, O.-H.; Kim, S.; Park, S.; Choi, M.-G.; Cha, M.; Park, S. Y.; Jang, D.-J. Imidazole-Based Excited-State Intramolecular Proton-Transfer Materials: Synthesis and Amplified Spontaneous Emission from a Large Single Crystal. *J. Am. Chem. Soc.* **2005**, *127*, 10070−10074.
(25) Francke, R.; Little, R. D. Optimizing Electron Transfer Mediators Based on Arylimidazoles by Ring Fusion: Synthesis, Electrochemistry, and Computational Analysis of 2-Aryl-1-methylphenanthro[9,10-d]imidazoles. *J. Am. Chem. Soc.* **2014**, *136*, 427−435.
(26) Padhy, A. K.; Chetia, B.; Mishra, S.; Pati, A.; Iyer, P. K. Imidazole derivatives as the Organic Precursor of ZnO Nano Particle. *Tetrahedron Lett.* **2010**, *51*, 2751−2753.
(27) Kumar, D.; Kommi, D. N.; Bollineni, N.; Patel, A. R.; Chakraborti, A. K. Catalytic Procedures for Multicomponent Synthesis of Imidazoles: Selectivity Control During the Competitive Formation of Tri- and Tetrasubstituted imidazoles. *Green Chem.* **2012**, *14*, 2038−2049.
(28) Kuzmenko, I.; Rapaport, H.; Kjaer, K.; Als-Nielsen, J.; Weissbuch, I.; Lahav, M. M.; Leiserowitz, L. Design and Characterization of Crystalline Thin Film Architectures at the Air−Liquid Interface: Simplicity to Complexity. *Chem. Rev.* **2001**, *101*, 1659−1696.
(29) McCullough, D. H.; Grygorash, R.; Hsu, J. T.; Regen, S. L. Insight into the Permeation Barrier of Glued Langmuir−Blodgett Bilayers. *J. Am. Chem. Soc.* **2007**, *129*, 8663−8667.
(30) Zasadzinski, J. A.; Viswanathan, R.; Madsen, L.; Garnaes, J.; Schwartz, D. K. Langmuir-Blodgett Films. *Science* **1994**, *263*, 1726−1733.
(31) Punkka, E.; Rubner, M. F. Molecular Heterostructure Devices Composed of Langmuir-Blodgett Films of Conducting Polymers. *J. Electron. Mater.* **1992**, *21*, 1057−1063.
(32) Reitzel, N.; Greve, D. R.; Kjaer, K.; Howes, P. B.; Jayaraman, M.; Savoy, S.; McCullough, R. D.; McDevitt, J. T.; Bjørnholm, T. Self-Assembly of Conjugated Polymers at the Air/Water Interface. Structure and Properties of Langmuir and Langmuir−Blodgett Films of Amphiphilic Regioregular Polythiophenes. *J. Am. Chem. Soc.* **2000**, *122*, 5788−5800.
(33) Hussain, S.-A.; Bhattacharjee, D. Langmuir-Blodgett Films and Molecular Electronics. *Mod. Phys. Lett. B* **2009**, *23*, 3437−3451.
(34) Gaines, G. L., Jr. *Insoluble Monolayers at Liquid−Gas Interfaces*; Interscience: New York, 1966.
(35) Sakakibara, K.; Hill, J. P.; Ariga, K. Thin-Film-Based Nanoarchitectures for Soft Matter: Controlled Assemblies into Two-Dimensional Worlds. *Small* **2011**, *7*, 1288−1308.
(36) Ulman, A. *An Introduction to Ultrathin Organic Films-From Langmuir-Blodgett to Self-Assembly*; Academic Press: Boston, 1991.
(37) Chen, X.; Lenhert, S.; Hirtz, M.; Lu, N.; Fuchs, H.; Chi, L. Langmuir−Blodgett Patterning: a Bottom-Up Way to Build Mesostructures Over Large Areas. *Acc. Chem. Res.* **2007**, *40*, 393−401.
(38) Tao, A. R.; Huang, J.; Yang, P. Langmuir−Blodgettry of Nanocrystals and Nanowires. *Acc. Chem. Res.* **2008**, *41*, 1662−1673.
(39) Zhang, R.; Xing, R.; Jiao, T.; Ma, K.; Chen, C.; Ma, G.; Yan, X. Carrier-Free, Chemophotodynamic Dual Nanodrugs via Self-Assembly for Synergistic Antitumor Therapy. *ACS Appl. Mater. Interfaces* **2016**, *8*, 13262−13269.
(40) Xing, R.; Jiao, T.; Liu, Y.; Ma, K.; Zou, Q.; Ma, G.; Yan, X. Co-Assembly of Graphene Oxide and Albumin/Photosensitizer Nanohybrids towards Enhanced Photodynamic Therapy. *Polymers* **2016**, *8*, 181.
(41) Liu, Y.; Ma, K.; Jiao, T.; Xing, R.; Shen, G.; Yan, X. Water-Insoluble Photosensitizer Nanocolloids Stabilized by Supramolecular Interfacial Assembly towards Photodynamic Therapy. *Sci. Rep.* **2017**, *7*, 42978−42986.
(42) Xing, R.; Liu, K.; Jiao, T.; Zhang, N.; Ma, K.; Zhang, R.; Zou, Q.; Ma, G.; Yan, X. An Injectable Self-Assembling Collagen−Gold Hybrid Hydrogel for Combinatorial Antitumor Photothermal/Photodynamic Therapy. *Adv. Mater.* **2016**, *28*, 3669−3676.
(43) Zhao, X.; Ma, K.; Jiao, T.; Xing, R.; Ma, X.; Hu, J.; Huang, H.; Zhang, L.; Yan, X. Fabrication of Hierarchical Layer-by-Layer Assembled Diamond-based Core-Shell Nanocomposites as Highly Efficient Dye Absorbents for Wastewater Treatment. *Sci. Rep.* **2017**, *7*, 44076−44089.
(44) Gao, P.; Liu, M. Compression Induced Helical Nanotubes in a Spreading Film of a Bolaamphiphile at the Air/Water Interface. *Langmuir* **2006**, *22*, 6727−6729.
(45) Liu, X.; Wang, T.; Liu, M. Interfacial Assembly of Cinnamoyl-Terminated Bolaamphiphiles Through the air/water Interface: Headgroup-Dependent Assembly, Supramolecular Nanotube and Photochemical Sewing. *Phys. Chem. Chem. Phys.* **2011**, *13*, 16520−16529.
(46) Yao, P.; Wang, H.; Chen, P.; Zhan, X.; Kuang, X.; Zhu, D.; Liu, L. Hierarchical Assembly of an Achiral π-Conjugated Molecule into a Chiral Nanotube through the Air/Water Interface. *Langmuir* **2009**, *25*, 6633−6636.
(47) Shankar, B. V.; Patnaik, A. Surface Pressure Driven Supramolecular Architectures from Mixed H-Aggregates of Dye-Capped Azobenzene Derivative. *Langmuir* **2006**, *22*, 4758−4765.
(48) Liu, L.; Hong, D.-J.; Lee, M. Chiral Assembly from Achiral Rod−Coil Molecules Triggered by Compression at the Air−Water Interface. *Langmuir* **2009**, *25*, 5061−5067.
(49) Jiao, T.; Liu, M. Supramolecular Assemblies of a New Series of Gemini-Type Schiff Base Amphiphiles at the Air/Water Interface: In Situ Coordination, Interfacial Nanoarchitectures, and Spacer Effect. *Langmuir* **2006**, *22*, 5005−5012.
(50) Jiao, T.; Liu, M. Substitution Controlled Molecular Orientation and Nanostructure in the Langmuir−Blodgett Films of a Series of Amphiphilic Naphthylidene-Containing Schiff Base Derivatives. *J. Colloid Interface Sci.* **2006**, *299*, 815−822.
(51) Jiao, T.; Li, X.; Zhang, Q.; Duan, P.; Zhang, L.; Liu, M.; Luo, X.; Li, Q.; Gao, F. Interfacial Assembly of a Series of Trigonal Schiff Base Amphiphiles in Organized Molecular Films. *Colloids Surf., A* **2012**, *407*, 108−115.
(52) Jiao, T.; Li, X.; Zhang, Q.; Li, Q.; Zhou, J.; Gao, F. Interfacial Assembly of a Series of Cu(II)-Coordinated Schiff Bases Complexes: Orderly Nanostructures and Supramolecular Chirality. *Sci. China: Technol. Sci.* **2013**, *56*, 20−24.
(53) Jiao, T.-F.; Liu, M.-H. Phase Behaviors and 2D-3D Morphological Transition of Aromatic Schiff Base Derivatives in Organized Molecular Films. *Acta Phys.-Chim. Sin.* **2012**, *28*, 1418−1424.
(54) Yuan, J.; Liu, M. Chiral Molecular Assemblies from a Novel Achiral Amphiphilic 2-(Heptadecyl) Naphtha[2,3]imidazole through Interfacial Coordination. *J. Am. Chem. Soc.* **2003**, *125*, 5051−5056.
(55) Boehm, C.; Leveiller, F.; Jacquemain, D.; Moehwald, H.; Kjaer, K.; Als-Nielsen, J.; Weissbuch, I.; Leiserowitz, L. Packing Characteristics of Crystalline Monolayers of Fatty Acid Salts, at the Air-Solution Interface, Studied by Grazing Incidence X-ray Diffraction. *Langmuir* **1994**, *10*, 830−836.
(56) Chen, P.; Ma, X.; Zhang, Y.; Hu, K.; Liu, M. Nanofibers and Nanospirals Fabricated through the Interfacial Organization of a Partially Fluorinated Compound. *Langmuir* **2007**, *23*, 11100−11106.
(57) Rubinger, C. P. L.; Moreira, R. L.; Cury, L. A.; Fontes, G. N.; Neves, B. R. A.; Meneguzzi, A.; Ferreira, C. A. Langmuir−Blodgett and

DOI: 10.1021/acs.langmuir.7b01750
Langmuir 2017, 33, 8383−8394

Langmuir−Schaefer Films of Poly(5-amino-1-naphthol) Conjugated Polymer. *Appl. Surf. Sci.* **2006**, *253*, 543−548.
(58) Barros, A. M.; Dhanabalan, A.; Constantino, C. J. L.; Balogh, D. T.; Oliveira, O. N., Jr. Langmuir Monolayers of Lignins Obtained with Different Isolation Methods. *Thin Solid Films* **1999**, *354*, 215−221.
(59) Liu, X.; Wang, T.; Liu, M. Interfacial Assembly of a Series of Cinnamoyl-Containing Bolaamphiphiles: Spacer-Controlled Packing, Photochemistry, and Odd−Even Effect. *Langmuir* **2012**, *28*, 3474−3482.
(60) Popovitz-Biro, R.; Majewski, J.; Margulis, L.; Cohen, S.; Leiserowitz, L.; Lahav, M. Self-Aggregation of α,ω-Alkanediols into 3-D Crystallites As Studied at Interfaces: The System of α,ω-Docosanediol. *J. Phys. Chem.* **1994**, *98*, 4970−4972.
(61) Masuda, M.; Shimizu, T. Multilayer Structure of an Unsymmetrical Monolayer Lipid Membrane with a 'Head-to-Tail' Interface. *Chem. Commun.* **2001**, *23*, 2442−2443.
(62) Debnath, P.; Chakraborty, S.; Deb, S.; Nath, J.; Bhattacharjee, D.; Hussain, S. A. Reversible Transition between Excimer and J-Aggregate of Indocarbocyanine Dye in Langmuir−Blodgett (LB) Films. *J. Phys. Chem. C* **2015**, *119*, 9429−9441.
(63) Sato, Y.; Furuki, M.; Tian, M.; Iwasa, I.; Pu, L. S.; Tatsuura, S. Improvement of On/Off Ratio in Single-Shot Multichannel Demultiplexing by using an Optical Kerr Gate of a Squarylium Dye J aggregate Film. *Appl. Phys. Lett.* **2002**, *80*, 2254−2256.
(64) Trivedi, M. K.; Branton, A.; Trivedi, D.; Nayak, G.; Saikia, G.; Jana, S. Physical and Structural Characterization of Biofield Treated Imidazole Derivatives. *Nat. Prod. Chem. Res.* **2015**, *3*, 187.
(65) Chakraborty, C.; Rana, U.; Pandey, R. K.; Moriyama, S.; Higuchi, M. One-Dimensional Anhydrous Proton Conducting Channel Formation at High Temperature in a Pt(II)-Based Metallo-Supramolecular Polymer and Imidazole System. *ACS Appl. Mater. Interfaces* **2017**, *9*, 13406−13414.
(66) Zou, L.; You, A.; Song, J.; Li, X.; Bouvet, M.; Sui, W.; Chen, Y. Cation-Induced Self-Assembly of an Amphiphilic Perylene Diimide Derivative in Solution and Langmuir−Blodgett films. *Colloids Surf., A* **2015**, *465*, 39−46.
(67) Nalwa, H. S. *Hand Book of Surfaces and Interfaces of Materials*; Academic Press: San Diego, U.S.A., 2001.
(68) Debnath, P.; Chakraborty, S.; Deb, S.; Nath, J.; Dey, B.; Bhattacharjee, D.; Hussain, S. A. Stability of J-aggregated Species in an Indocarbocyanine Dye in Langmuir−Blodgett Films. *J. Lumin.* **2016**, *179*, 287−296.
(69) Chakraborty, S.; Bhattacharjee, D.; Soda, H.; Tominaga, M.; Suzuki, Y.; Kawamata, J.; Hussain, S. A. Temperature and Concentration Dependence of J-aggregate of a Cyanine Dye in a Laponite Film Fabricated by Langmuir−Blodgett Technique. *Appl. Clay Sci.* **2015**, *104*, 245−251.
(70) Hussain, S. A.; Deb, S.; Biswas, S.; Bhattacharjee, D. Langmuir−Blodgett Films of 9-Phenyl anthracene Molecules Incorporated into Different Matrices. *Spectrochim. Acta, Part A* **2005**, *61*, 2448−2454.
(71) Zhang, X.; Shen, J. Self-Assembled Ultrathin Films: From Layered Nanoarchitectures to Functional Assemblies. *Adv. Mater.* **1999**, *11*, 1139−1143.
(72) Yuan, Y.; Chen, J.-X.; Lu, F.; Tong, Q.-X.; Yang, Q.-D.; Mo, H.-W.; Ng, T.-W.; Wong, F.-L.; Guo, Z.-Q.; Ye, J.; Chen, Z.; Zhang, X.-H.; Lee, C.-S. Bipolar Phenanthroimidazole Derivatives Containing Bulky Polyaromatic Hydrocarbons for Nondoped Blue Electroluminescence Devices with High Efficiency and Low Efficiency Roll-Off. *Chem. Mater.* **2013**, *25*, 4957−4965.
(73) Skonieczny, K.; Ciuciu, A. I.; Nichols, E. M.; Hugues, V.; Blanchard-Desce, M.; Flamigni, L.; Gryko, D. T. Bright, Emission Tunable Fluorescent Dyes Based on Imidazole and π-Expanded Imidazole. *J. Mater. Chem.* **2012**, *22*, 20649−20664.
(74) Zhang, Y.; Lai, S.-L.; Tong, Q.-X.; Chan, M.-Y.; Ng, T.-W.; Wen, Z.-C.; Zhang, G.-Q.; Lee, S.-T.; Kwong, H.-L.; Lee, C.-S. Synthesis and Characterization of Phenanthroimidazole Derivatives for Applications in Organic Electroluminescent Devices. *J. Mater. Chem.* **2011**, *21*, 8206−8214.
(75) Bandyopadhyay, A.; Pal, A. J. Large Conductance Switching and Memory Effects in Organic Molecules for Data-Storage Applications. *Appl. Phys. Lett.* **2003**, *82*, 1215−1217.
(76) Liu, G.; Ling, Q.-D.; Kang, E.-T.; Neoh, K.-G.; Liaw, D.-J.; Chang, F.-C.; Zhu, C.-X.; Chan, D. S.-H. Bistable Electrical Switching and Write-Once Read-Many-Times Memory Effect in a Donor-Acceptor Containing Polyfluorene Derivative and its Carbon Nanotube Composites. *J. Appl. Phys.* **2007**, *102*, 024502−024508.
(77) Bandyopadhyay, A.; Pal, A. J. Key to Design Functional Organic Molecules For Binary Operation with Large Conductance Switching. *Chem. Phys. Lett.* **2003**, *371*, 86−90.
(78) Wang, Q.; Masao, I.; Tan, M.; Dai, P.; Wu, Y.; Lu, S.; Yang, H. High Quality Non-Rectifying Contact of ITO with Both Ni and n-type GaAs. *J. Semicond.* **2015**, *36*, 053003.
(79) Tahar, R. B. H.; Ban, T.; Ohya, Y.; Takahashi, Y. Tin doped indium oxide thin films: Electrical properties. *J. Appl. Phys.* **1998**, *83*, 2631−2645.
(80) Chu, C. W.; Ouyang, J.; Tseng, J.-H.; Yang, Y. Organic Donor−Acceptor System Exhibiting Electrical Bistability for Use in Memory Devices. *Adv. Mater.* **2005**, *17*, 1440−1443.
(81) Song, Y.; Ling, Q. D.; Lim, S. L.; Teo, E. Y. H.; Tan, Y. P.; Li, L.; Kang, E. T.; Chan, D. S. H.; Zhu, C. Electrically Bistable Thin-Film Device Based on PVK and GNPs Polymer Material. *IEEE Electron Device Lett.* **2007**, *28*, 107−110.
(82) Potember, R. S.; Poehler, T. O.; Cowan, D. O. Electrical Switching and Memory Phenomena in Cu-TCNQ Thin Films. *Appl. Phys. Lett.* **1979**, *34*, 405.
(83) Kamitsos, E. I.; Tzinis, C. H.; Risen, W. M. Raman Study of the Mechanism of Electrical Switching in Cu TCNQ Films. *Solid State Commun.* **1982**, *42*, 561−565.

DOI: 10.1021/acs.langmuir.7b01750
Langmuir 2017, 33, 8383−8394